Title

Demonstration of waferscale voltage amplifier and electrostatic quadrupole focusing array for compact linear accelerators

Journal

Journal of Applied Physics, 125(19)

ISSN

0021-8979

Authors

Vinayakumar, KB
Ardanuc, S
Ji, Q
et al.

Publication Date

2019-05-21

DOI

10.1063/1.5091979

Peer reviewed

Demonstration of waferscale voltage amplifier and electrostatic quadrupole focusing array for compact linear accelerators

K. B. Vinayakumar[1,a)], S. Ardanuc[1], *Q. Ji[2], A. Persaud[2], P. Seidl[2], T. Schenkel[2] and A. Lal[1]*

[1]SonicMEMS Laboratory, Cornell University, Ithaca, New York 14853, USA

[2]E. O. Lawrence Berkeley National Laboratory, 1 Cyclotron Road, Berkeley, California 94720, USA

a) Corresponding author, *vinayjgi@gmail.com*

Abstract:

Compact linear accelerators with beam energies in the keV to MeV range have applications in medicine, neutron/X-ray generation, surface modifications, etc. The size, weight and power of existing accelerators precludes them from mass availability in portable formats. This paper presents a specific implementation of an ion accelerator architecture based on planar wafers with accelerating and focusing sections. Our low cost approach allows the control of the final ion beam energy with potential applications, for example, for accelerator-based ion implantation. In this paper, we demonstrate two important waferscale modules required to build a linear particle accelerator these include (1) on-wafer voltage amplification for beam acceleration using Inductor-Capacitor (LC) resonators and (2) waferscale electrostatic quadrupole arrays (ESQA) to re-focus the ion beams during transport. On-board LC resonators were developed using a Printed Circuit Board (PCB) fabrication processes to implement an LC element resonant at ~16.6 MHz with a quality factor of 25. An energy gain of ~250 electron volts was observed using a two wafer acceleration unit with an argon ion beam with 6.5 keV initial energy. A 3×3 ESQA was fabricated on a glass wafer with metal electrodes formed by depositing copper metal around the beam apertures. The ESQA was used to focus and defocus an argon ion beam demonstrating a field gradient of ~500 V over a gap of ~250 microns.

Index Terms— Linear RF accelerators, LC resonators, Electrostatic Quadrupole (ESQ), Ion beam.

I. INTRODUCTION

Compact linear accelerators, producing ions in the keV to MeV energy range have a variety of applications ranging from biomedical treatment and surface treatment to ion beam drivers for fusion [1, 2]. In most of the applications there is a demand for portable, low cost, high efficiency accelerators [1-3]. Most of the commercially available accelerators use a single ion beam [1, 4,

and 5]. A large single ion beam requires high electric/magnetic fields to focus the ion beam during beam transport. Furthermore, the space-charge repulsion limits the maximal transportable beam current. Hence, it is difficult to achieve high current-densities in small footprint single beam accelerators. In this paper, a Multiple Electrostatic Quadrupole Array Linear Accelerator (MEQALAC) concept has been adopted to reduce the space-charge issues and improve the effective current density by relying on multiple beamlets [6]. Furthermore, this approach lends itself to reduce the total power required during acceleration and focusing [6]. Maschke et al. in 1979 demonstrated the first MEQALAC concept using electrostatic focusing electrodes and showed that the beam current density scales favorable for smaller beam apertures [6]. Later, in 1989 Urbanus et al. demonstrated the MEQALAC using four He^+ ion beams of 2.2 mA per channel with channel diameter of 2.5 mm [7]. Due to the use of conventional machining, where relatively large gaps had to be applied to achieve uniform beams due to the manufacturing tolerances, both aforementioned MEQALAC concepts were limited by the achievable beam aperture diameter. In addition, the previous approaches used RF cavity resonators to accelerate the ion beams, and this led to increases in the total size of the accelerator. By utilizing modern fabrication methods we can now dramatically reduce these critical dimension and take better advantage of the scaling laws for this approach.

Fig. 1 shows the concept of the wafer-based MEQALAC design used in this work. In general, the main components required to build a MEQALAC are an ion source, accelerating and focusing stages. In our recently published work, RF accelerating stages and beam focusing stages were demonstrated to build a compact MEQALAC [8]. Here, the RF accelerating wafers were fabricated by routing metal on FR4 and an external LC resonator circuit was used to drive high voltages on the RF wafers at frequencies around 15 MHz and to accelerate multiple ion beams in parallel [8]. Using this external resonator (voltage amplifier), an accelerator consisting of six accelerating gaps was demonstrated [9]. The external resonators will increase the size, power and cost of a complete accelerator system. The better approach is to directly integrate the high-voltage generation on the wafer. In the present work, we demonstrated an on-wafer voltage amplification scheme generating the accelerating electric fields directly near the acceleration gaps greatly reducing stray capacitances from cables needed to otherwise deliver the high voltage.

In addition to the accelerating fields, another important component required to build a wafer-based MEQALAC is the ESQA (ElectroStatic Quadrupole Array). ESQA are used to re-focus the ion beams along the beam line, correcting for any spread due to space-charge forces [1, 2]. To study the performance of the fabrication tolerance, robustness and breakdown issues of ESQA, in our previous work we demonstrated micromachined silicon, 3D-printed plastic, and PCB based approaches for ESQAs [8, 10, 11]. PCB ESQAs were fabricated using laser machining and sidewall metal deposition techniques [8]. Due to the laser fabrication, dimensional tolerances and sidewall roughness in the order of 10 micrometers, limit the accuracy with which the focusing parameters can be controlled. Furthermore, in PCB-based ESQA the polymer (FR4) outgassing rate can potentially effect the beam quality. Silicon ESQAs have the advantage of very good dimensional tolerance and sidewall roughness owing to the use of lithographic techniques with sub-micron precision. However, silicon processing can be time consuming to develop, and less resilient to shocks because silicon is brittle [10]. Recently, we reported on the ion beam focusing ability of a nickel coated 3D-printed monomer resins as an ESQA [11]. This approach, however, resulted in worse uniformity compared to other approaches and increased potential for outgassing. To provide good mechanical stability, high electrostatic field gradients, and low outgassing rates in this work, we explore the possibility of fabricating ESQA using glass wafers. Advantages and disadvantages of different ESQA approaches are listed in Table 1.

To summarize, in this paper we demonstrate two alternative implementations required to build a waferscale MEQALAC. The first component demonstrated is an on-wafer voltage amplification concept using a LC resonator. The on-board inductor was fabricated on Rogers PCboard to achieve smaller RF loss in the PC board. To form the desired LC circuit, a capacitor/inductor wafer and ground wafer were assembled using precision washers. Using this planar inductor followed by a vertically integrated capacitor, a voltage amplification has been observed by accelerating an ion beams. The second component demonstrated is a glass-wafer ESQA to focus the ion beams. We describe the design and fabrication of the glass ESQA and show results on focusing of multiple argon ion beams.

II. Principle of Operation

A) LC-resonator based accelerating structure

The planar structure used for accelerating consists of two wafers where the gap between the wafers contains the accelerating field. For an electrical model the gap can be modeled as a pure capacitor. In our implementation this capacitance is driven through an inductor fabricated on one of the wafers to achieve a high voltage through the voltage gain of a series LC tank circuit operating at resonance. Fig. 2A shows the schematic sketch of the assembled waferscale LC resonator, where an inductor wafer and a ground wafer are separated using precision washers to form a capacitor region. Fig. 2B shows the circuit diagram of the setup where the output voltage of the resonator across the capacitor is Quality factor (~Q) times the input RF voltage. Fig. 2C shows the electric field region in the LC resonator structure, where the acceleration of the ion/particle beam occurs due to the potential difference between the ground wafer and the inductor wafer. For the experimental ion beam acceleration setup, a double acceleration gap concept was used, where two acceleration gaps were driven using a single RF source [8]. Fig. 3 shows the 2D and 3D view of the assembled LC resonator structure with two acceleration gaps and a drift region in the middle. Two inductor wafers were placed facing away from each other to minimize the mutual inductance effect and ground wafers were assembled using precision washers to form the acceleration gaps. As we see from Fig. 3A, ions see ground potential when entering and leaving the acceleration unit cell, so that many accelerating stages can be cascaded. The acceleration gap is designed to be 10% of the drift region (d). For a given ion beam energy the length of the drift region was calculated using equation (1) [8].

$$d = \frac{\beta\lambda}{2} \qquad (1)$$

where λ is the RF wavelength, $\beta = v/c$, with ion velocity, v, and speed of light, c, d is the center to center distance between adjacent acceleration gaps consisting of the wafer thickness and the length of the drift region. Equation (1) ensures that the RF phase is suchs that ions being accelerated in the first gap are also accelerated when arriving at the second acceleration gap.

B) ESQ focusing wafer

The ESQ structure requires a positive and a negative high voltage electrode. The high voltages have to be isolated using an insulating material, in this case consisting of glass. Fig. 4A shows the glass based ESQ structure. Here, metal electrodes are inserted into the glass wafer using a glass etching and metal electroplating process, described in the fabrication section. The metal electrodes

are encased in glass and not placed at the edge of the orifice, due to constraints of the fabrication process. The field generated across electrodes is not hindered by the glass dielectric, but the glass needs to be taken into account during the design stage. Fig. 4(A1) shows a round beam entering an ESQ with no potential applied on the electrodes therefore leading to no effects on the beam. Fig. 4(A2) and Fig. 4(A3) show the effect of the ESQs on a positively charged ion beam during application of voltages of alternative polarity on the electrodes resulting in beam focusing in one direction and defocusing in the other. The electrostatic forces on the positive ions will be repulsive towards positive electrodes and attractive towards negative electrodes. This results in an elliptical beam shape for an initial round beam. Combining two ESQs and placing them with a rotation of 90 degrees with respect to each other, allows for an overall focusing effect [8, 11]. Fig. 4B shows a COMSOL model of an electrostatic field distribution in an ESQ. Fig. 4C shows the simulated electric field distribution on the x and y axis of an ESQ. For an ideal ESQ, the electric field at the center should be zero and the field should increase linearly towards the electrodes (Fig. 4C). As can be seen in the simulations, the fields show the as expected approximately linear relationship. The electric field in this architecture also extends in the glass area having a higher dielectric constant of ~3.9. This effectively can be compared to a glass and a vacuum capacitor in series, reducing the maximum possible field that can be achieved in the vacuum section of the ESQ.

III. Device fabrication and testing

a) The LC resonator fabrication

Fig. 2 and Fig. 3 show the concept of waferscale LC-resonator sketch and the experimental setup used to achieve LC resonator based voltage amplification. On-wafer inductors were formed by patterning the metal on top of the PCB insulating substrate (Fig. 5) and capacitors were formed by assembling a pair of a ground wafer and an inductor wafer using precision washers. To achieve a high Q a Rogers board (RT 5880) with low loss tangent (0.0004) was used to fabricate both the inductor and ground wafers. We used a standard PCB fabrication process to fabricate inductor and ground wafers (Fig. 5). The fabrication process was started with double sided Rogers boards. Orifices are formed for the ion beam/particles to move through using a laser cutter. Next, the front side metal was patterned to form an inductor. Similarly, the metal on the opposite wafer side was patterned to reduce high electric field regions and stray capacitance. The ground wafer was fabricated using a similar approach. Fig. 6A shows the fabricated inductor wafer, ground wafer and assembled LC resonator structure and Fig. 6B shows their impedance and phase characteristics

measured using a network analyzer. The resonant peak and the zero crossing of the phase were observed at a frequency of ~16.6 MHz with a quality factor of ~30. We measured on board inductor and capacitor values of 1.55 μH and 17.08 pF, respectively.

B) ESQ fabrication Process

Glass is used as the insulating substrate and Through-Glass-Vias (TGV) are used to form the electrodes. Glass based TGV are used commercially for electronics applications such as semiconductor packaging, 3D-IC stacking, fanout wafer level packaging etc [12]. This approach allows fabrication on a low cost substrate with smaller features than what might be possible with PCB [8]. Furthermore, the very good vacuum compatibility of glass and its high breakdown voltages are advantageous to obtain high field gradients. The basic steps of the process flow are illustrated in Fig. 7. The process was started by forming through holes using laser machining. Then parts of the holes are filled with a conductive slurry/epoxy through stencil masking and then cured. After cleaning/polishing, top and bottom metallization are done using physical vapor deposition and/or electroplating. This process was developed in collaboration with Triton Microtechnologies company.

Fig. 8A shows the fabricated 3×3 glass ESQA with metal routing to connect positive and negative electrodes. The zoomed-in version of a single ESQ shows the aperture area (~0.5 mm) for the ion beams with top and bottom electrode routing. The measured electrical breakdown voltage for the fabricated glass ESQA in air and vacuum is more than 1 kV with > 1 MOhm resistance. Fig. 8B shows the schematic of 3×3 ESQA cross section with apertures to focus the ion beams.

IV. EXPERIMENTAL SETUP FOR ION ACCELERATION

The cross sectional schematic of the ion source and the ion extraction unit are shown in Fig. 9A. Fig. 9B shows the assembled LC wafers before mounting inside the vacuum chamber (with alignment holes in-line with the ion beam extraction unit). A filament-driven multi-cusp ion-extraction system was used to test the waferscale amplifier to accelerate the ion beams and to test the glass ESQA to focus the ion beams [13]. To achieve a stable plasma in the ion source the filament was driven with several amperes of current over several seconds and beam was extracted during a ~300 μsec pulse with a continuous argon gas flow. During the filament arc pulse, ions were extracted from the plasma using a three electrode system. During all experiments the plasma

facing electrode was floating. The second electrode was biased with a negative voltage relative to the source. The third electrode can be used to achieve shorter pulses, but for the experiments reported here was always biased slightly above the second electrode potential with the same polarity and therefore had no effect on the beam extraction. After the negatively biased third electrode, ions are accelerated toward the ground electrode and gain kinetic energy. As discussed in the aforementioned sections, the current study is focused on accelerating multiple parallel beams simultaneously to archive high current density in a compact setup. Hence, as a prototype, a 3×3 beam aperture-based extraction system was used with 0.5 mm beam apertures and with center to center distance of 5 mm between the each aperture.

Following extraction from the ion source, we used either the LC resonator assembly to accelerate the ion beam or a glass ESQA to focus the 3×3 array of ion beams. For the LC resonator test, the structure consisting of two acceleration gaps and one drift region (Fig. 3) was used. The drift region and acceleration gap were designed to match the injection energy of the argon ion beams of 6.5 keV. The drift region was adjusted in such a way that the RF voltage phase changed by 180 degrees when the ions entered the second acceleration gap. Before mounting the wafers into the vacuum chamber, a bench test was carried out to find the resonance frequency and quality factor (voltage gain) of the fabricated LC resonators using a high voltage probe and the longer cables needed to connect the setup inside the vacuum chamber. Fig. 10A shows the measured voltages from the RF power amplifier and LC resonator at different frequencies. A voltage gain of ~30 was observed at 22.7 MHz from the LC resonator during a bench test/ion beam test. The resonance frequency during the bench test/ion beam is different compared to the resonance frequency measured using the network analyzer. This is due the fact that the long wires and the vacuum chamber will introduce extra capacitance and inductance into the resonant circuit. This in turn will shift the resonance frequency and reduce the quality factor of the LC resonator. Fig. 10B shows the voltages used at the different amplification stages during the ion beam test from the external function generator and RF amplifier (manufactured by ENI) and the on-board LC resonator. A 200 mV input voltage (peak-to-peak) at 22.7 MHz was used from the external RF function generator, which was connected in series with an RF power amplifier. After the RF power amplifier, a voltage of ~10 V (peak-to-peak) was obtained at 22.7MHz. This 10 V voltage at 22.7MHz was then used to drive the on-board LC resonator. Fig. 9A shows the accelerator setup, where the fabricated waferscale LC resonator assembly is placed in-line with the beam extraction unit followed by a

retarding grid assembly and a Faraday cup used to measure the ion current above a given ion kinetic energy [8]. The bias on the retarding grid was scanned and from the measured decrease of the ion beam current in the Faraday cup one can calculate ion beam energy distribution. First a measurement without applied RF was taken to confirm the initial ion energy and then a measurement with RF voltages applied was used to measure the energy gain due to acceleration in the two acceleration gaps where RF high voltages were generated by the LC-resonators**.** A voltage gain of ~25 was observed from the fabricated LC resonator during the ion beams test and the resulting kinetic energy gain is plotted in Fig .11. Apart from particle accelerator, the waferscale high gain radio frequency resonators developed in the present work have potential application in developing waferscale EPR/NMR spectroscopies [14-17].

In a similar experiment the ion source and ion extraction system was used to test the ESQA (Fig. 9A). Here, the accelerating wafers and Faraday cup were replaced by glass ESQAs and a scintillator (RP 400 plastic scintillator) together with a fast image intensifying camera (Princeton instruments) [9]. After mounting the ESQA, the positive and negative bias on the ESQA electrodes were swept to observe the focusing/defocusing effect. Fig. 12 shows the captured focusing and defocusing images using the image intensifying camera for a bias voltage of ±200V on the ESQA electrodes. The fabricated ESQA had a resistance of >1 MOhm and a leakage current of ~0.1 mA during initial beam tests. This leakage current is likely due to current paths due to leftover metal slurry, and could be reduced in the future.

V. RESULTS AND DISCUSSION

Ion beams were extracted in a 3×3 array from a multi-cusp ion source [8] and injected into the wafer structure where ions were accelerated by the RF high voltages generated with the on-board LC resonators. Fig. 11 shows the increase of the ion energy from the initial energy of 6.5 keV to an energy of 6.75 keV. Here, acceleration was driven by two acceleration gaps (Fig. 9A) with locally generated RF voltages from the on-board LC resonators. An acceleration of 125V/gap at 22.7 MHz was observed, in total an increase of 250 V ion kinetic energy was observed in a two stage acceleration setup. The measurement also shows some ions losing kinetic energy which is due to ions arriving at the wrong phase of the RF. In a final acceleration implementation one would only inject ions during the correct phase or bunch the beam before injection to avoid this problem. The voltage gain factor or quality factor achieved from the fabricated LC resonator during ion

beam test is ~25 and this can be further improved by designing a better impedance matching circuit between the LC resonator and RF amplifiers. Also, the quality factor can be improved by reducing metal losses, dielectric losses and tangent loss in the wafer-scale resonators.

We then conducted beam focusing tests with a 3×3 array of glass ESQA. Fig. 12 shows the measured beam focusing and defocusing effects. Argon ions with a beam energy of 12 keV were used to demonstrate focusing effects. Light from the ion source filament interfered with the camera images during beam spot measurements and we had to block four of the nine beam apertures to reduce the interference from ion source light emission, leaving a set of five beams. Fig. 12A shows the ion beams when there is no electric potential applied on the ESQA. Fig. 12B and Fig. 12C shows focusing and defocusing of positive argon beams when voltages of ± 200V were applied on the ESQA. One can cleary see the elongated beam spots when a voltage is applied and that the focusing direction changes when the polarity is flipped. To achieve an overall focusing effect in both direction one would mount two ESQAs that are rotated 90 degree in respect to each other [8, 11].

VI. CONCLUSIONS AND OUTLOOK

In this work we have demonstrated waferscale approaches to implement components for a multi-beam accelerator. We have implemented acceleration units consisting of on-wafer LC resonators and glass ESQA to focus ion beams. The developed on-board resonators to amplify voltage locally shows a very promising result for the development of very compact waferscale accelerators. During the beam test a voltage amplification of ~25 per acceleration gap was obtained using on-board LC resonators. We discussed routes to further increase the voltage amplification and acceleration gradient from currently 125 V/gap. We also note that the on-board LC-circuits we describe here can be combined with near-board sources for high RF acceleration voltages for specific applications. The developed glass ESQAs also shows very promising results to hold high voltage of more than ~1kV in air and vacuum that enable efficient re-focusing and transport of ions in a compact, low cost linear accelerator. Our results show a path forward to build an integrated wafer scale compact linear accelerators that is fully compatible with silicon batch fabrication processes for massive scaling at low cost. A next step will be the integration of

acceleration and focusing stages to form a complete wafer based MEQALAC with high beam current (scaled by the number of beams) and high ion energy (scaled by the number of acceleration stages) for applications in basic and applied science and industrial processes.

ACKNOWLEDGEMENTS: This work was supported by the Office of Science of the U.S. Department of Energy through the ARPA-E ALPHA program under Contract No. DE-AC0205CH11231. Device fabrication was carried out at the Cornell Nano Fabrication (CNF) facility, a member of the National Coordinate Science Foundation (NNCI) network, supported by the National Science Foundation (Grant No. ECCS-1542081).

References:

1. Hamm, Robert Wray, and Marianne Elizabeth Hamm, eds. Industrial accelerators and their applications. World Scientific, 2012.
2. Wangler, Thomas P. RF Linear accelerators. John Wiley & Sons, 2008.
3. Hasan, SM Shajedul, Yoon W. Kang, and Mostofa K. Howlader. "Development of an RF Conditioning System for Charged-Particle Accelerators." IEEE Transactions on Instrumentation and Measurement 57, no. 4 (2008): 743-750.
4. Bryant, P. J. "A brief history and review of accelerators." (1991).
5. Kumar, Sandeep, Haeryong Yang, and Heung-Sik Kang. "Beam dynamics study of a 30 MeV electron linear accelerator to drive a neutron source." Journal of Applied Physics 115.6 (2014): 064510.
6. Maschke, A. W. Space-charge limits for linear accelerators. No. BNL-51022. Brookhaven National Lab., Upton, NY (USA), 1979.
7. Urbanus, W. H., R. G. C. Wojke, J. G. Bannenberg, H. Klein, A. Schempp, R. W. Thomae, T. Weis, and P. W. Van Amersfoort. "MEQALAC: A 1-MeV multichannel rf-accelerator for light ions." *Nuclear Instruments and Methods in Physics Research Section B: Beam Interactions with Materials and Atoms* 37 (1989): 508-511.
8. Persaud, A., Q. Ji, E. Feinberg, P. A. Seidl, W. L. Waldron, T. Schenkel, A. Lal, K. B. Vinayakumar, S. Ardanuc, and D. A. Hammer. "A compact linear accelerator based on a scalable microelectromechanical-system RF-structure." *Review of Scientific Instruments* 88, no. 6 (2017): 063304.

9. Persaud, A., P. A. Seidl, Q. Ji, E. Feinberg, W. L. Waldron, T. Schenkel, S. Ardanuc, K. B. Vinayakumar, and A. Lal. "Staging of RF-accelerating units in a MEMS-based ion accelerator." *Physics Procedia* 90 (2017): 136-142.
10. Vinayakumar, K. B., A. Persaud, P. A. Seidl, Q. Ji, W. L. Waldron, T. Schenkel, S. Ardanuc, and A. Lal. "Waferscale Electrostatic Quadrupole Array for Multiple Ion Beam Manipulation." 2018 IEEE Micro Electro Mechanical Systems (MEMS)
11. Seidl, P. A., A. Persaud, W. Ghiorso, Q. Ji, W. L. Waldron, A. Lal, K. B. Vinayakumar, and T. Schenkel. "Source-to-accelerator quadrupole matching section for a compact linear accelerator." *Review of Scientific Instruments* 89, no. 5 (2018): 053302.
12. Shorey, Aric B., and Rachel Lu. "Progress and application of through glass via (TGV) technology." *Pan Pacific Microelectronics Symposium (Pan Pacific), 2016*. IEEE, 2016.
13. Ji, Q., P. A. Seidl, W. L. Waldron, J. H. Takakuwa, A. Friedman, D. P. Grote, A. Persaud, J. J. Barnard, and T. Schenkel. "Development and testing of a pulsed helium ion source for probing materials and warm dense matter studies." *Review of Scientific Instruments* 87, no. 2 (2016): 02B707.
14. Brand, Oliver, Gary K. Fedder, Christofer Hierold, and Osamu Tabata. *Micro and Nano Scale NMR: Technologies and Systems*. John Wiley & Sons, 2018.
15. Peng, Weng Kung, Lan Chen, and Jongyoon Han. "Development of miniaturized, portable magnetic resonance relaxometry system for point-of-care medical diagnosis." *Review of Scientific Instruments* 83, no. 9 (2012): 095115.
16. Sun, Nan, Tae-Jong Yoon, Hakho Lee, William Andress, Ralph Weissleder, and Donhee Ham. "Palm NMR and 1-chip NMR." *IEEE Journal of Solid-State Circuits* 46, no. 1 (2011): 342-352.
17. Peng, Weng Kung, Tian Fook Kong, Chee Sheng Ng, Lan Chen, Yongxue Huang, Ali Asgar S. Bhagat, Nam-Trung Nguyen, Peter Rainer Preiser, and Jongyoon Han. "Micromagnetic resonance relaxometry for rapid label-free malaria diagnosis." *Nature medicine* 20, no. 9 (2014): 1069.

Figure Captions:

Fig. 1. 3D schematic of the multi beam accelerator concept with ion source, accelerating resonators and focusing stages.

Fig. 2. High voltage generation across an acceleration gap using a wafer-based LC resonator (A) 3D view of the assembled LC resonator design (B) Schematic of the LC resonator (C) Cross section of the assembled LC resonator with electric field lines

Fig 3 (A) cross sectional view of the single acceleration unit cell using 4 wafers with two LC tank wafer unit. (B) 3D view of the assembled single acceleration unit cell

Fig.4. Electric field distribution of glass ESQ (A) Effect of electrode potential on the ion beam (B) COMSOL simulation of the electric field distribution in glass ESQ (C) Simulated electric field distribution in x and y axis shows the zero electric field at the center of the ESQ

Fig. 5. Fabrication procedure for RF wafers and ground wafers: (a) the process starts with a double side copper coated Rogers RT 5880 board that is cut in the shape of a 4 inch wafer. (b) Holes are formed into the board by laser drilling. (c) The top metal layer is patterned (inductor coil for inductor wafer and metal around aperture for ground wafer). (d) The bottom metal is patterned using alignment with fiducials.

Fig. 6. (A) Fabricated spiral inductor and ground wafer that form an LC-resonator. (B) Impedance and phase characteristics of the fabricated LC resonator show the resonance frequency and quality factor of the device. the holes on the edges were used to align the wafer structure on guide posts with the beam extraction unit.

Figure 7: Glass ESQA fabrication - laser micromachining and metal deposition technique.

Fig.8. (A) Fabricated glass ESQA with aperture and top and bottom metal routing; zoomed-in version on a single ESQ on the right (B) Cross section of the 3×3 ESQA with argon ion beam moving in ESQ aperture.

Fig. 9 (A) Experimental setup for beam tests. (B) Assembled LC-resonator for beam tests.

Fig.10. (A) Voltage gain during bench testing of the LC resonator at different frequency (B) Voltages obtained from function generator, external RF amplifier and LC resonator during bench test/ion beam test

Fig.11. Scans of ion current (Amperes) as a function of retarding grid bias showing ion energy gain due to acceleration by RF high voltages from on-board LC resonators. Argon ions were injected with a kinetic energy of 6.5 keV and we observed acceleration by 250 V in two acceleration gaps.

Fig. 12. Beam focusing and defocusing using glass ESQAs. The beam spots are 5 mm apart. Due to interference from light from the ion source filament, four beam spots had to be blocked.

Table Captions:

Table 1: Comparison of different ESQA performance with respect to their fabrication tolerance, voltage holding, mass fabrication compatibility and mechanical stability

Material	**Fabrication tolerance** (High to Low)	**Breakdown voltage** (High to Low)	**Mass fabrication** (Difficult to easy)	**Mechanical stability** (High to Low)
PCB [8]	High	Low	Difficult	Medium
Plastic [10]	Medium	Medium	Difficult	Medium
Silicon [11]	Low	Medium	Easy	Low
Glass (present work)	Medium	High	Difficult	High

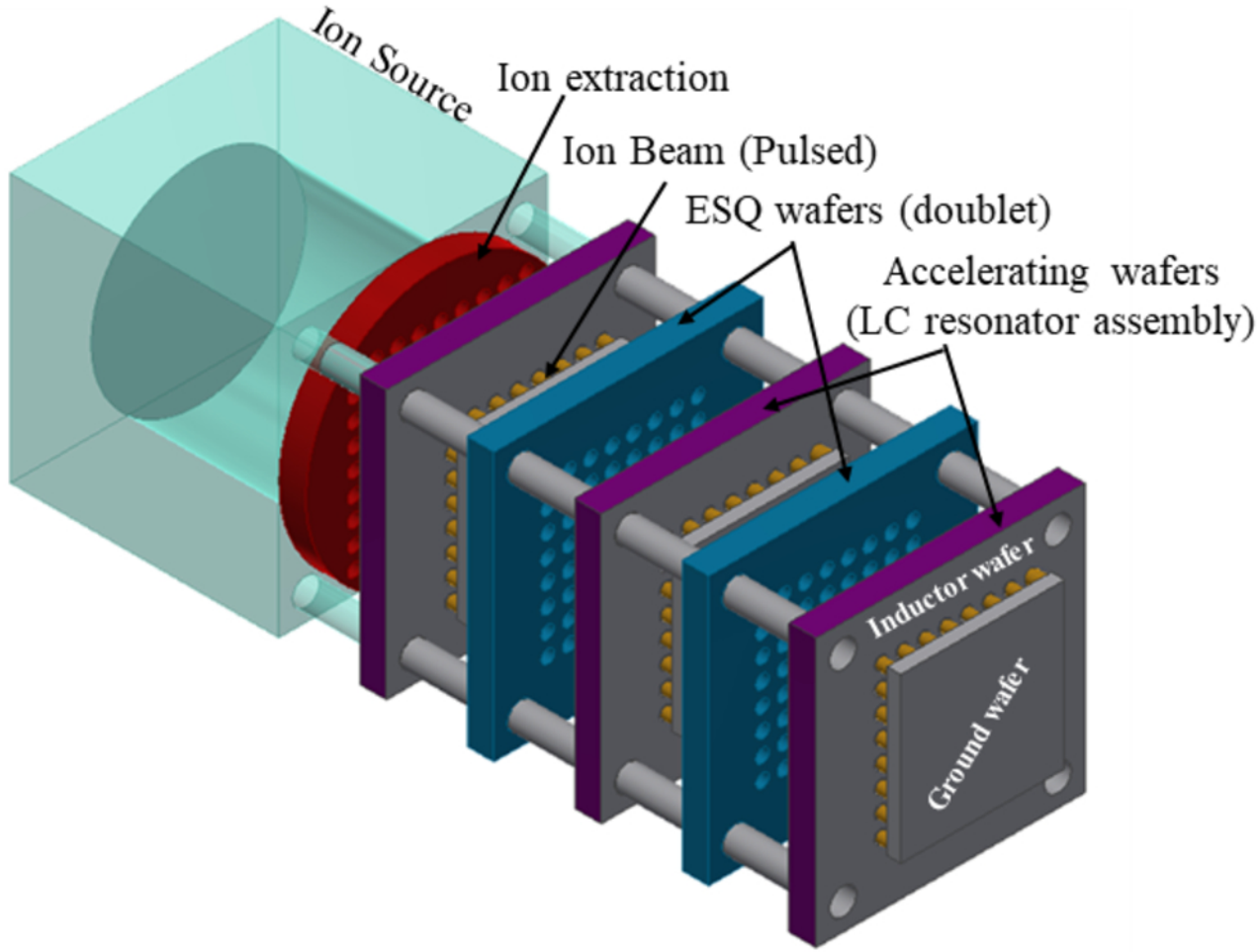
Ion Source
Ion extraction
Ion Beam (Pulsed)
ESQ wafers (doublet)
Accelerating wafers
(LC resonator assembly)
Inductor wafer
Ground wafer

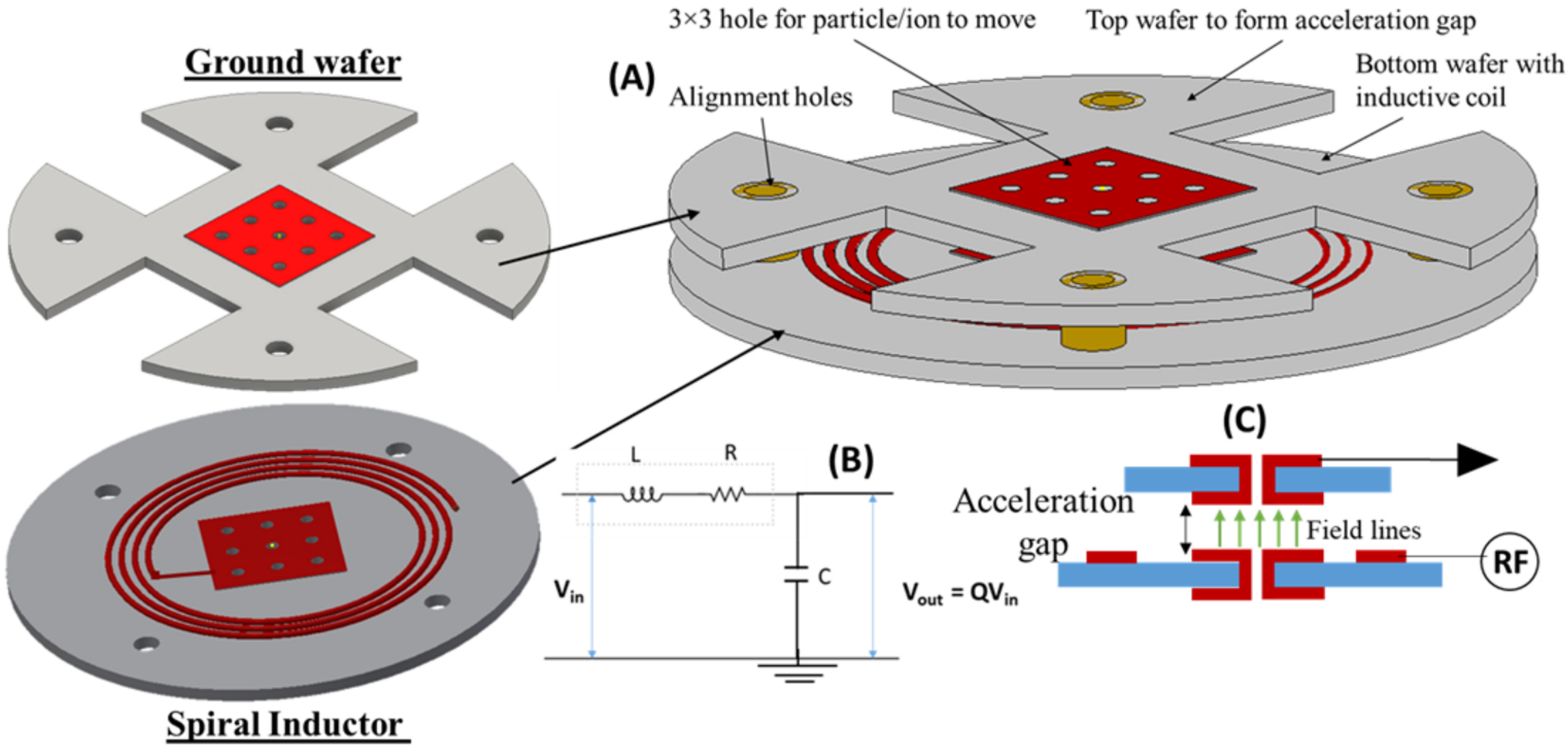
Ground wafer
Spiral Inductor
(A)
3×3 hole for particle/ion to move
Top wafer to form acceleration gap
Alignment holes
Bottom wafer with inductive coil
(B)
L
R
C
V_{in}
$V_{out} = QV_{in}$
(C)
Acceleration gap
Field lines
RF

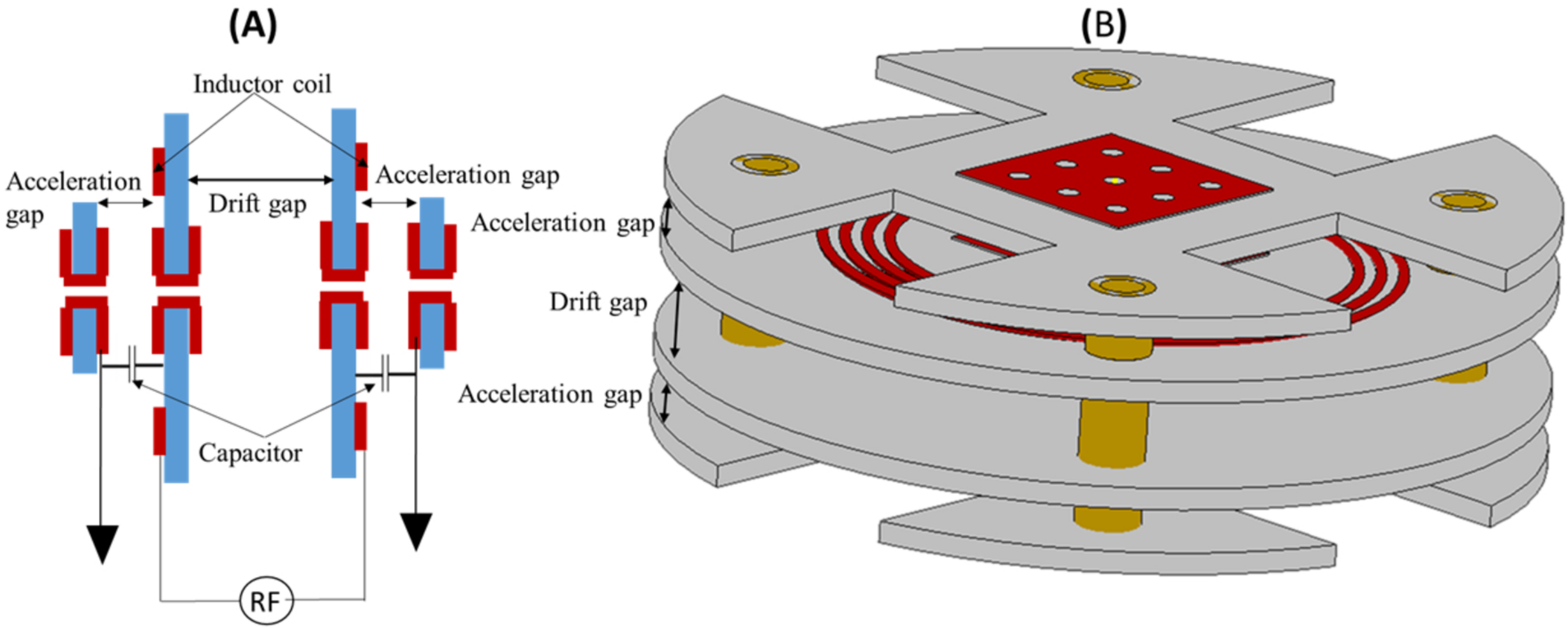
(A)
Inductor coil
Acceleration gap
Drift gap
Acceleration gap
Capacitor
RF
(B)
Acceleration gap
Drift gap
Acceleration gap

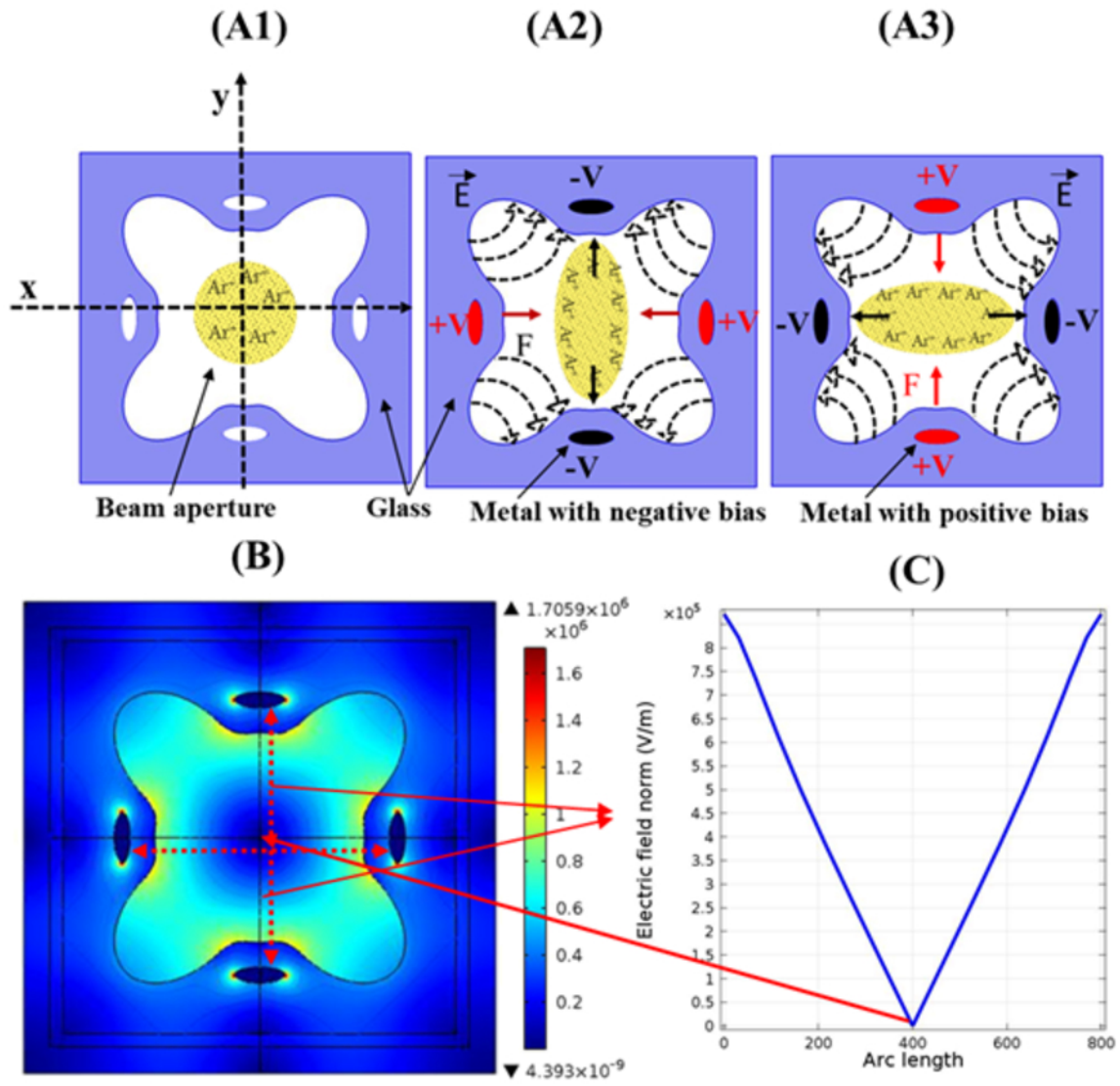
(A1)
(A2)
(A3)
y
x
E
-V
+V
F
Ar+
Beam aperture
Glass
Metal with negative bias
Metal with positive bias
(B)
(C)
▲ 1.7059×10^6
×10^6
1.6
1.4
1.2
1
0.8
0.6
0.4
0.2
▼ 4.393×10^-9
×10^5
Electric field norm (V/m)
Arc length
0
200
400
600
800

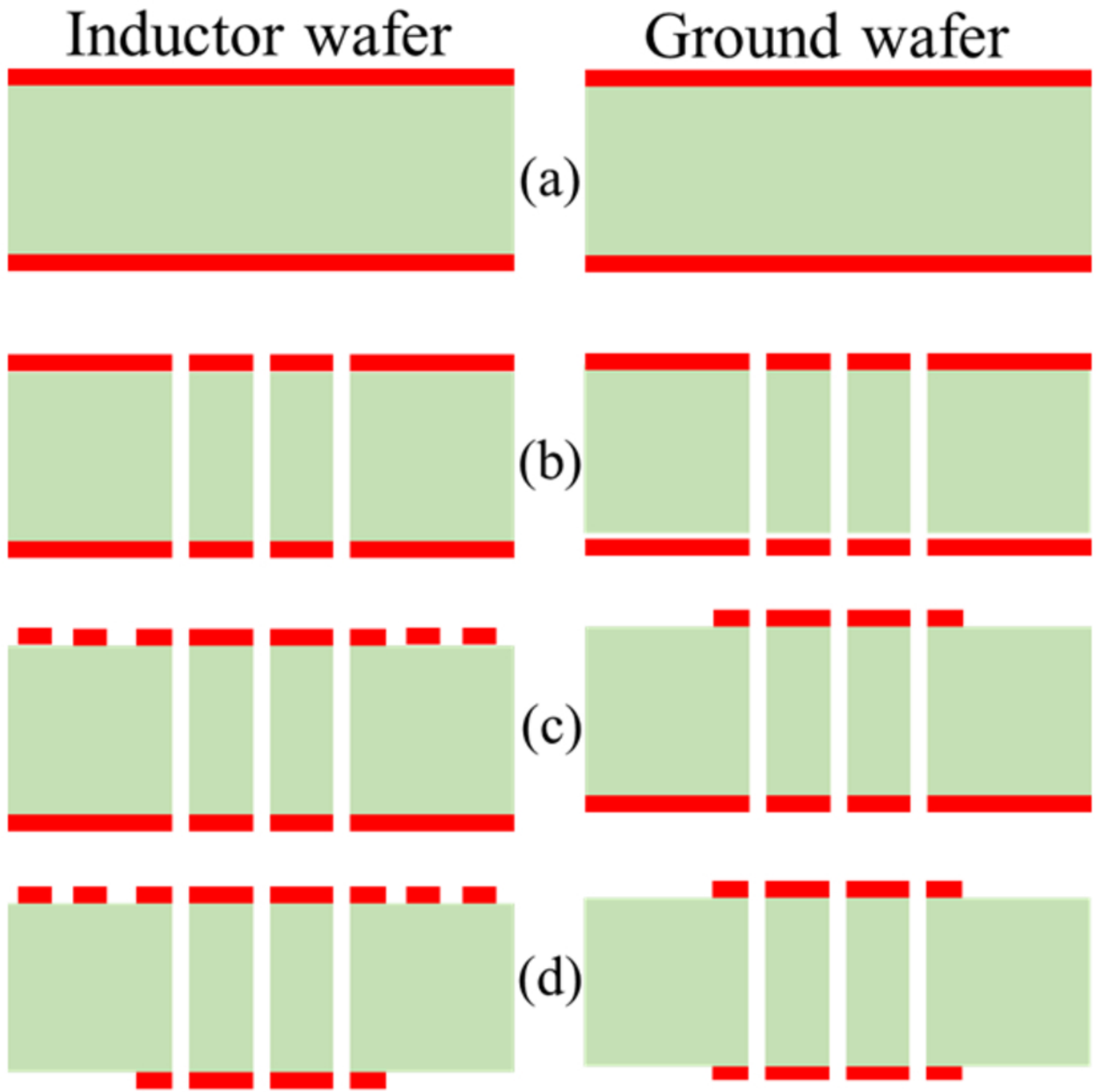
Inductor wafer
Ground wafer
(a)
(b)
(c)
(d)

(A)

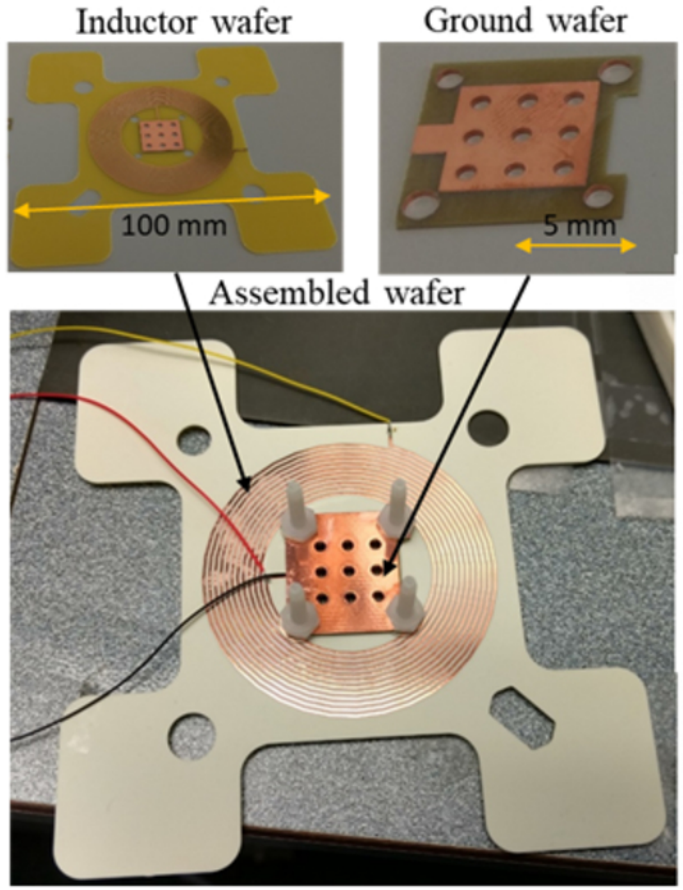
Inductor wafer
Ground wafer
100 mm
5 mm
Assembled wafer

(B)

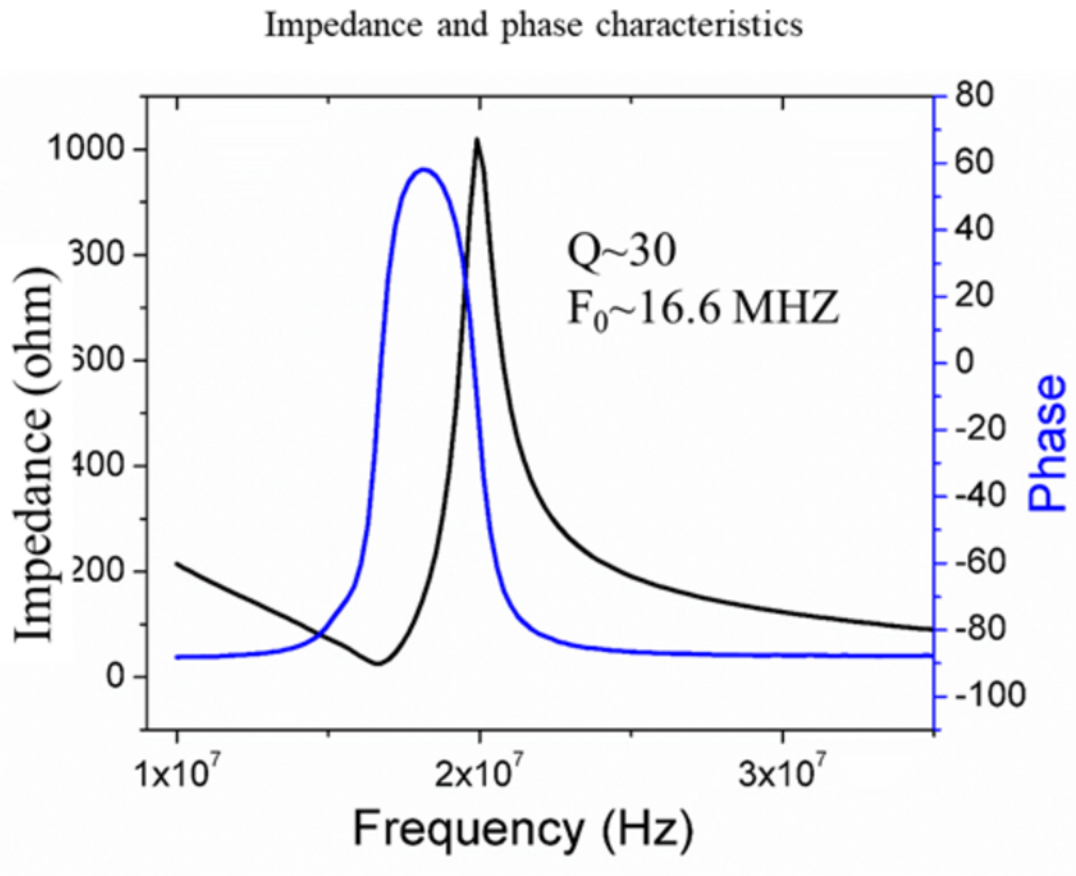
Impedance and phase characteristics
Q~30
F0~16.6 MHZ
Impedance (ohm)
Phase
Frequency (Hz)
1000
300
300
400
200
0
80
60
40
20
0
-20
-40
-60
-80
-100
1x10^7
2x10^7
3x10^7

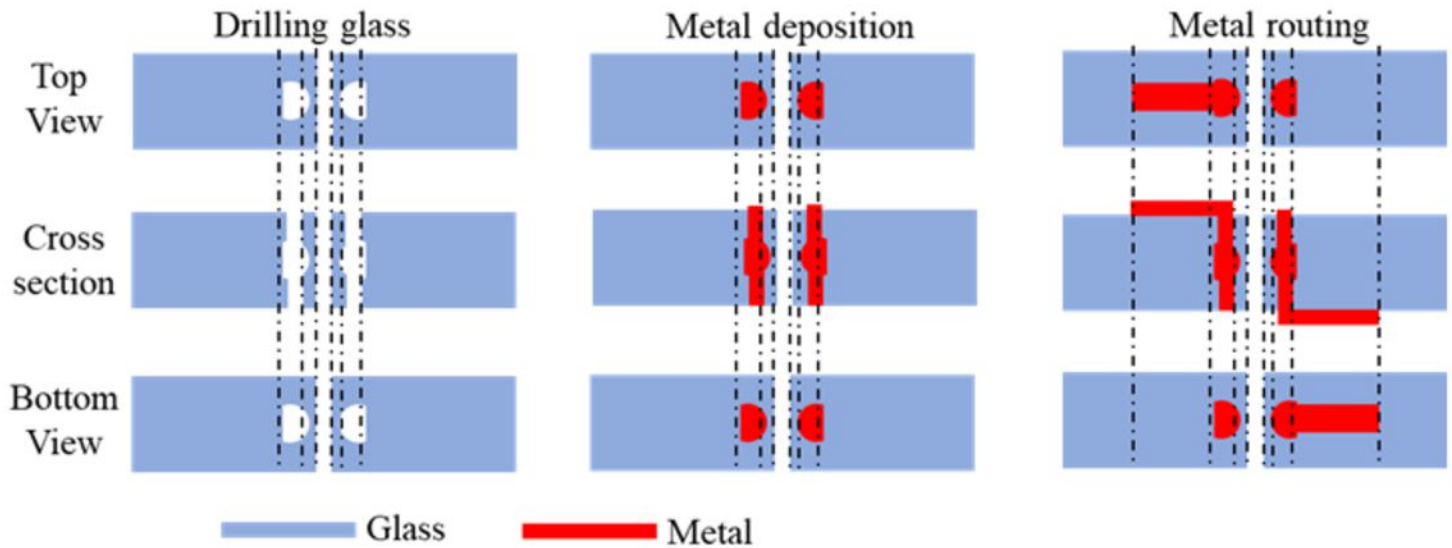
Drilling glass
Metal deposition
Metal routing
Top View
Cross section
Bottom View
Glass
Metal

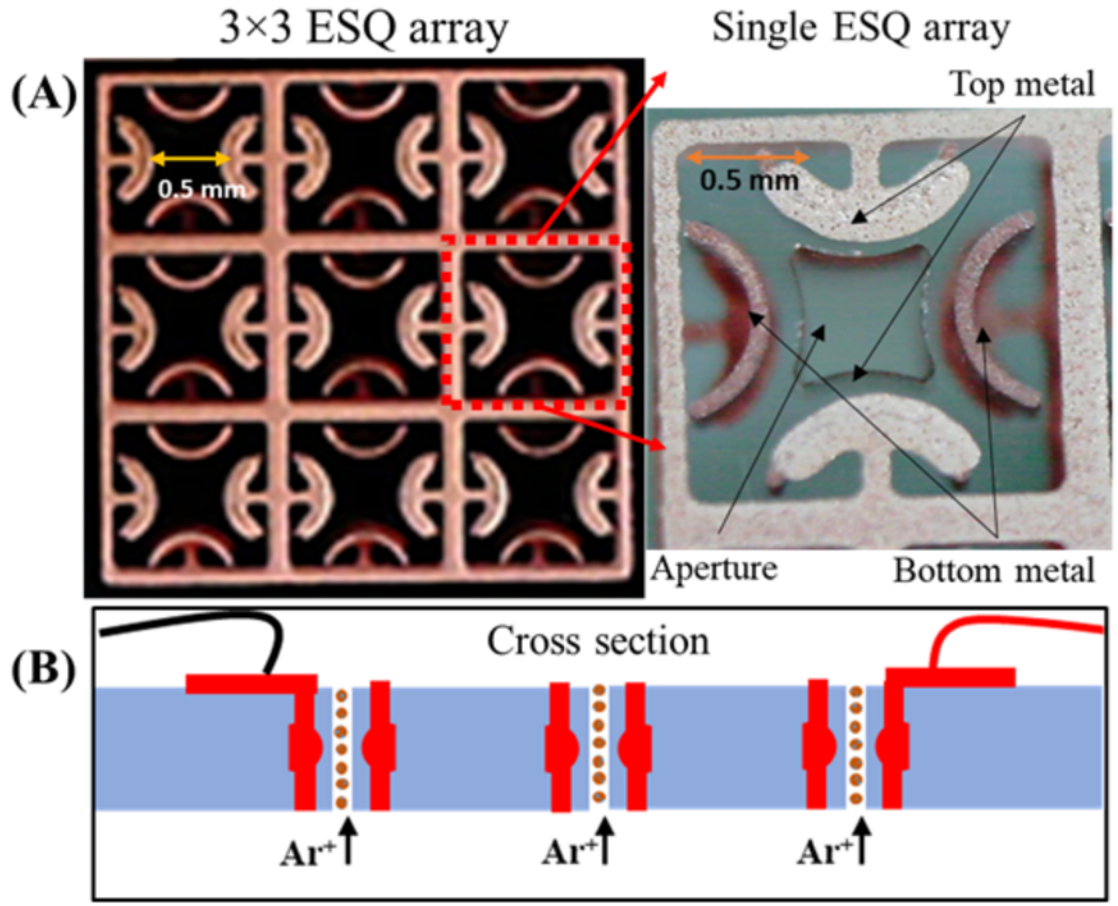
3×3 ESQ array
Single ESQ array
(A)
0.5 mm
Top metal
0.5 mm
Aperture
Bottom metal
(B)
Cross section
Ar+
Ar+
Ar+

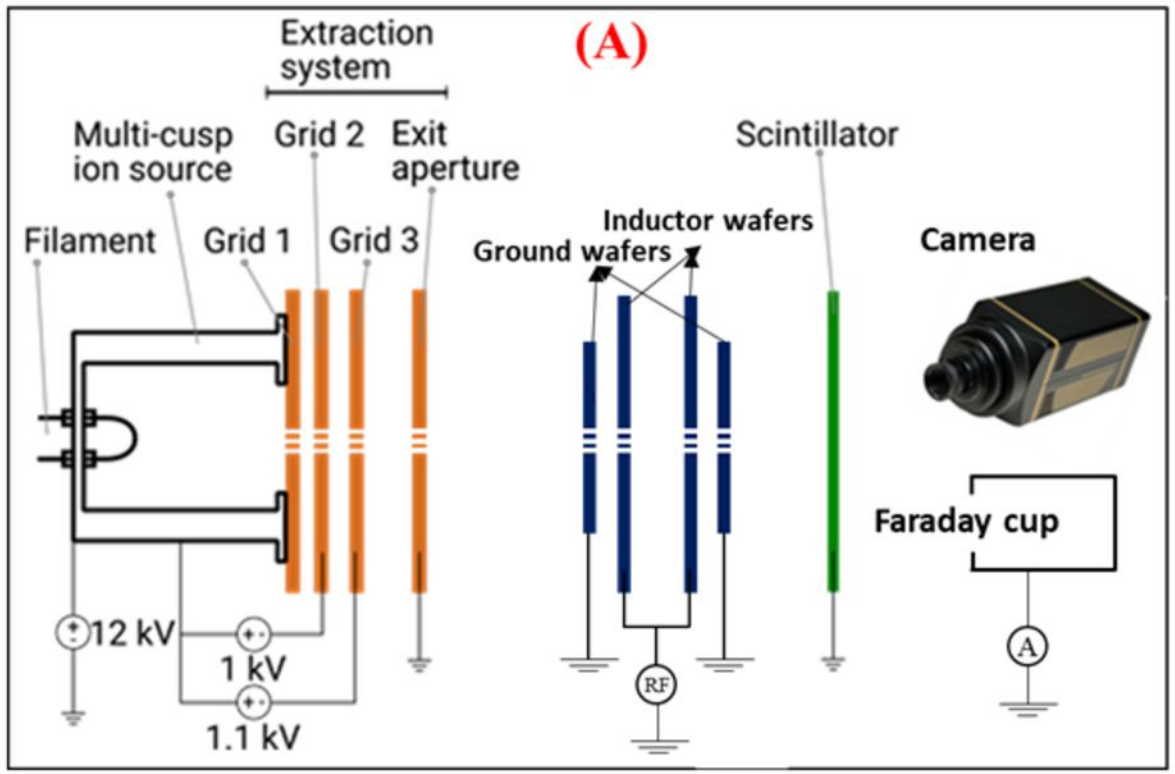
(A)
Extraction system
Multi-cusp ion source
Grid 2
Exit aperture
Scintillator
Filament
Grid 1
Grid 3
Inductor wafers
Ground wafers
Camera
Faraday cup
12 kV
1 kV
1.1 kV
RF
A

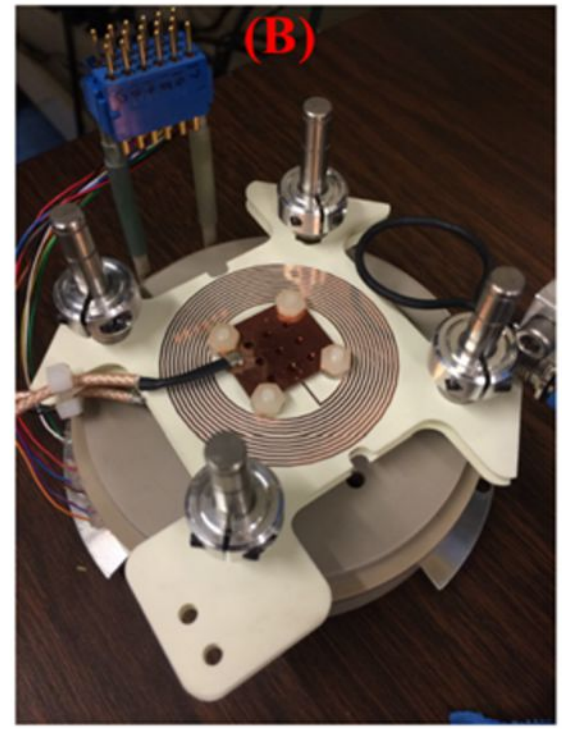
(B)

(A) Voltage gain at different frequency

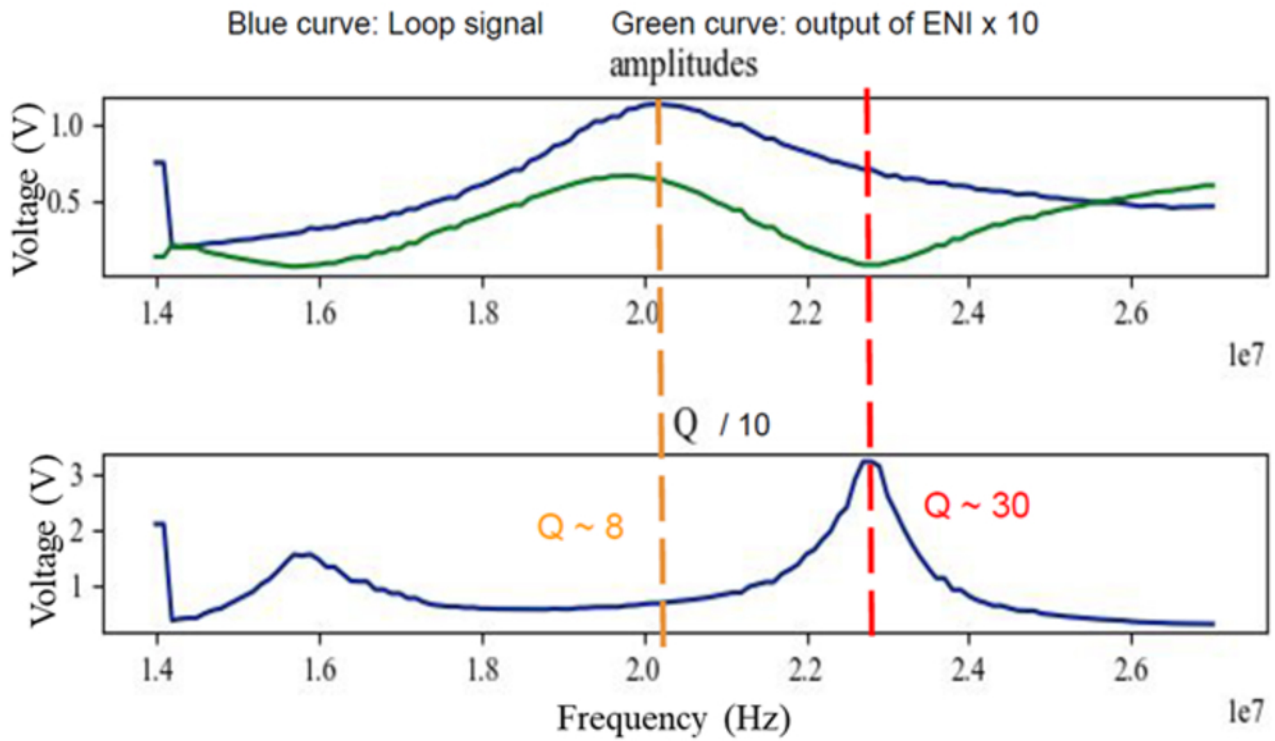

(B) Voltages during beam test

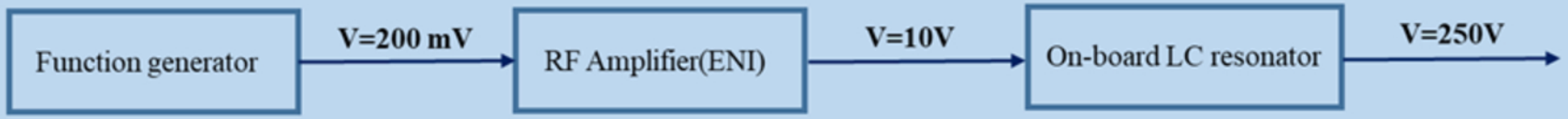

@22.7 MHz

Gain of 25/stage was observed with the beam test

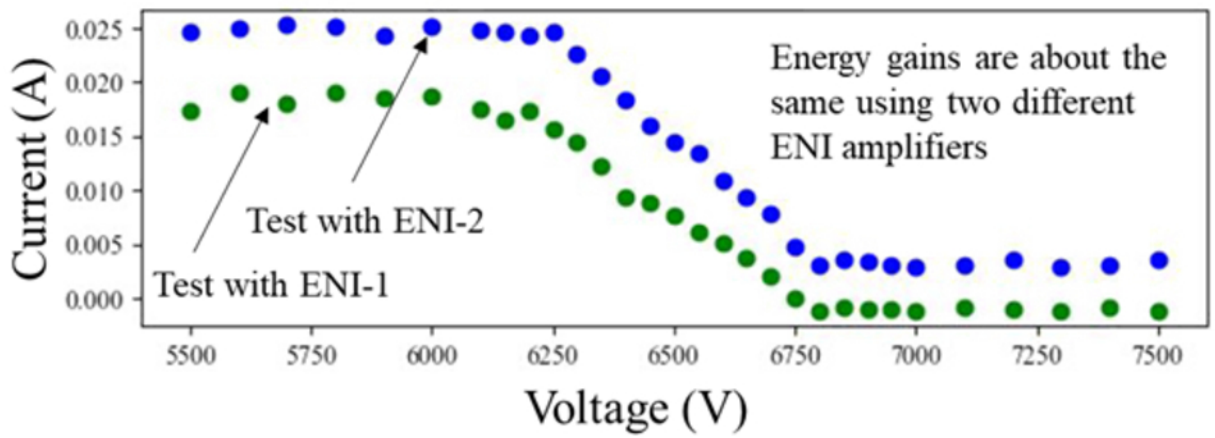
Current (A)
0.025
0.020
0.015
0.010
0.005
0.000
5500
5750
6000
6250
6500
6750
7000
7250
7500
Voltage (V)
Energy gains are about the same using two different ENI amplifiers
Test with ENI-2
Test with ENI-1

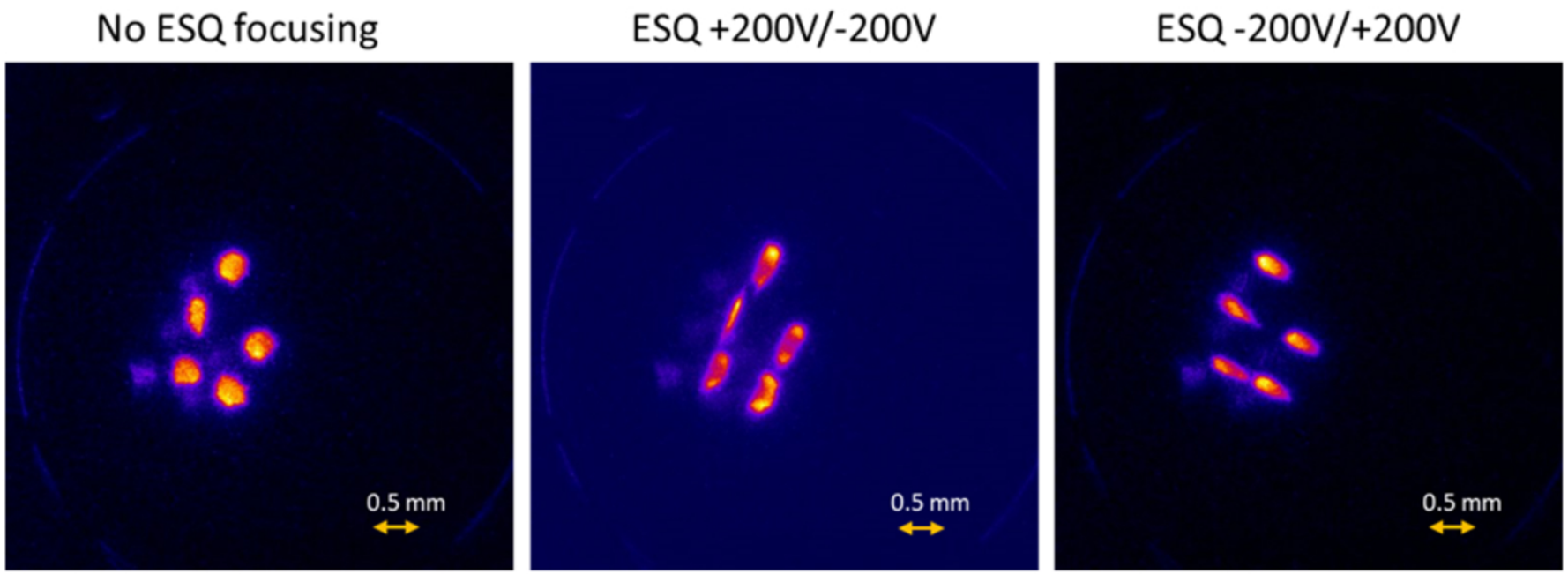
No ESQ focusing
ESQ +200V/-200V
ESQ -200V/+200V
0.5 mm
0.5 mm
0.5 mm